International Journal of Heat and Mass Transfer 52 (2009) 4296–4301

Contents lists available at ScienceDirect

International Journal of Heat and Mass Transfer

journal homepage: www.elsevier.com/locate/ijhmt

Thermal characterization of porous graphitic foam – Convection in impinging flow

K. Sultan [a], C.T. DeGroot [a], A.G. Straatman [a,*], N.C. Gallego [b], H. Hangan [c]

[a] Department of Mechanical and Materials Engineering, The University of Western Ontario, London, Ont., Canada N6A 5B9
[b] Materials Science and Technology Division, Oak Ridge National Laboratory, Oak Ridge, TN 37831-6087, USA
[c] Department of Civil and Environmental Engineering, The Boundary Layer Wind Tunnel Laboratory, The University of Western Ontario, London, Ont., Canada N6A 5B9

ARTICLE INFO

Article history:
Received 23 October 2008
Accepted 31 March 2009
Available online 23 May 2009

Keywords:
Graphitic foam
Convective heat transfer enhancement

ABSTRACT

An experimental study has been undertaken to explore the convective heat transfer enhancement that can be achieved in an impinging airflow arrangement by bonding layers of graphitic foam to a heated metal substrate. The effects of foam protrusion, foam thickness and foam properties were explored in this study. The results show that surfaces with a layer of foam protruding upward with open edges had the highest convective enhancement over that of the bare substrate under the same conditions. For the protruding cases, convective enhancements of 30-70% were observed for airflows ranging from 7-11 m/s, for foam thicknesses in the range 2-10 mm. The highest enhancements were observed for foam specimens with the most open, interconnected void structure.

1. Introduction

Porous graphitic foam (GF) is being investigated as a material to enhance heat transfer in an impinging flow arrangement. Developed by Oak Ridge National Laboratories (ORNL) [1,2], GF has several distinct advantages over the more traditional metallic foams such as those made from aluminum. For example, the effective conductivity of a typical GF is in the range 40–160 W/m K [2], whereas the effective conductivity of a typical aluminum foam is between 2 and 26 W/m K. This difference is mainly attributed to the significant differences in the conductivities of the constituent material; graphite has a material conductivity of 800–1900 W/m K, while typical aluminum alloys have material conductivities of 140–237 W/m K. The high effective conductivity of GF is coupled with an open, interconnected void structure that exposes a large internal surface area (5000–50,000 m^2/m^3 [1]) for convective heat transfer.

To obtain maximum heat transfer, the fluid must be forced through the foam so that it is exposed to the internal surface area. However, in many cases a forced-flow configuration is impractical due to the very high pressure drop that can occur [3]. Recently, Straatman et al. [4] investigated the heat transfer characteristics of GF in parallel flow. In their experiments, a layer of foam was bonded to a solid substrate and subjected to airflow across the foam surface. In this arrangement, convective enhancement occurs due to the roughness of the exposed surface as well as that due to infiltration of the fluid into the foam surface. The fluid that penetrates the foam does so at a very modest pressure drop so heat transfer enhancement comes at a very low cost. Enhancements of 30–10% were measured over the range of Reynolds numbers 100,000–500,000. Experimental work was also carried out by Jayman and Mohamad [5] in which a heated cylinder was fitted with low-porosity graphitic foam fins and subjected to air in a cross-flow arrangement. Because of the low-porosity of the graphitic foam fins, heat transfer was mainly due to flow around the fins. The reported heat transfer was not superior to that achieved using an array of aluminum fins since the internal area of the foam was not accessible to the air stream.

This paper aims to extend the characterization work of Straatman et al. [3,4] by reporting measurements of the thermal performance of GF in an impinging flow arrangement. Previous work on impinging flow on a porous media has been conducted by [6–8] using metal reticulated foams. In their experiments, airflow was passed through the surface of a cylindrical foam block that was bonded to a metal substrate. The impinging airflow was passed through a sleeve that was fit tightly to the foam surface such that all of the airflow was forced to pass into the surface. As such, the arrangement was closer to a forced-flow than an impinging flow. In the present investigation the flow is unconstrained, so the fluid can either pass through or around the foam. The objective is to quantify the enhancement in convective heat transfer due to the natural infiltration of air into the surface of different graphitic foam specimens. The remaining sections of the paper describe the GF specimens tested, the experimental setup and procedure, and the results of the experiments.

2. Graphitic foam specimens

Three different GF specimens have been considered in the present work. These GF specimens were produced using the patented

* Corresponding author.
E-mail address: astraatman@eng.uwo.ca (A.G. Straatman).

0017-9310/$ - see front matter © 2009 Elsevier Ltd. All rights reserved.
doi:10.1016/j.ijheatmasstransfer.2009.03.070

foaming process [1] and supplied by POCO™ (221-1) and Oak Ridge National Laboratory (219-1 and 219-2). Information about the GF production process and the procedures followed to obtain their properties can be found in [1]. The relevant geometric properties and effective thermal conductivities of the specimens are summarized in Table 1. Scanning electron microscope (SEM) images of the foam specimens are given in Fig. 1. Two different parameters are given in Table 1 describing the void distribution of the GF specimens. While the average pore diameter is the most common parameter used, Straatman et al. [4] found that the highest frequency void diameter was often more useful for interpreting the pore level activity. Fig. 1 shows that the 221-1 specimen supplied by POCO™ has the most homogeneous void structure in terms of pore size. This is also reflected in Table 1 where the average and highest frequency void diameter are essentially the same. Fig. 1 shows that the 219-1 foam is comprised of mainly very large-diameter voids, but with several smaller voids in the substantial regions between the large voids. These small voids appear to be well-distributed in these regions, but may be isolated from the flow due to a lack of interconnectivity. In foams like this, the flow tends not to penetrate the smaller pores since the path of least resistance is through the substantially larger interconnected pore structure. As such, much of the internal area can go unused. The final image in Fig. 1 shows that the 219-2 foam is similar in structure to the 219-1 foam in that it is comprised of several pore diameters, but since the range of pore diameter is narrower than that in the 219-1 foam, it is expected that more of the internal surface area will be accessed by fluid flow.

The final column of Table 1 gives the effective conductivity of the foam specimens calculated using the relation given by [9], which uses the porosity, the pore diameter and the solid and fluid phase conductivities to produce an analytical estimate of k_{eff}. The effective conductivity is primarily a function of the porosity and the solid-phase conductivity. The 221-1 specimen has a slightly lower porosity than the other specimens, but a very high solid-phase conductivity (≈1640 W/m K), and thus a significantly higher effective conductivity. In comparison, the solid-phase conductivities of the ORNL specimens are ≈1300 (219-1) and ≈1400 W/m K (219-2).

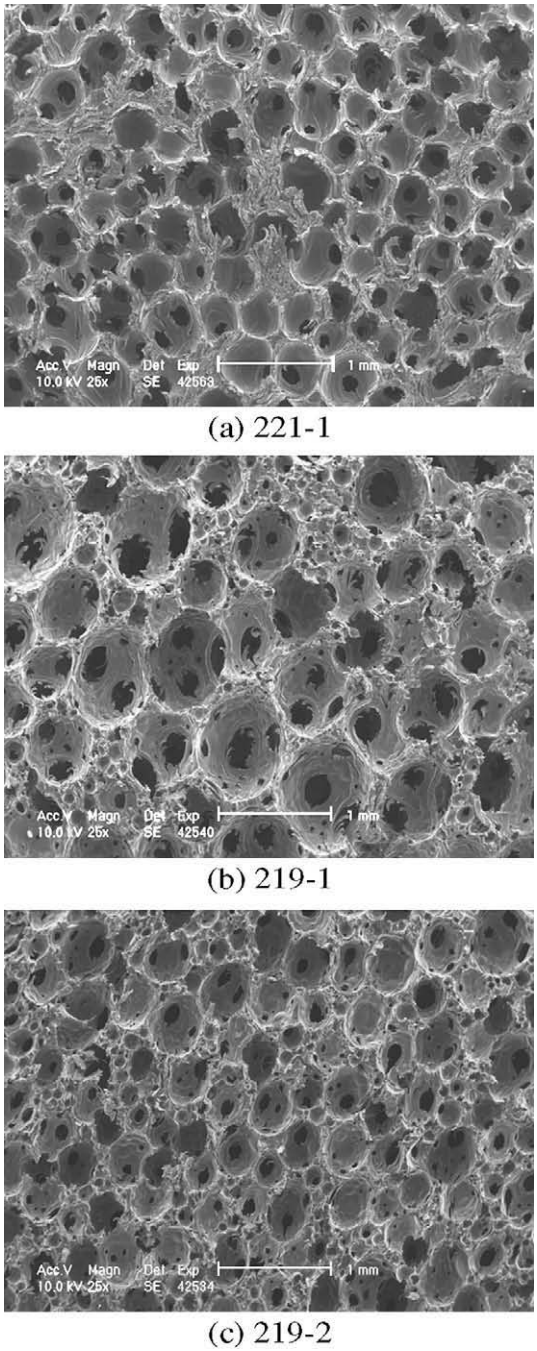

Fig. 1. Scanning Electron Microscope (SEM) images of the three foam specimens considered in the present work.

3. Theoretical basis

The Nusselt number is used to quantify the convective heat transfer from the surfaces exposed to air impingement:

$$Nu_D = \frac{hD}{k},$$

where h is the convective heat transfer coefficient, D is the diameter of the flat exposed surface, and k is the conductivity of air taken at the temperature of the exposed surface. The heat transfer is obtained experimentally from:

$$h = \frac{q}{A(T_p - T_\infty)},$$

where q is the electrical input energy, A is the plan area of the flat exposed surface, T_p is the surface temperature of the exposed surface, and T_∞ is the ambient temperature of the impinging air stream. The condition of the impinging air stream is characterized by Reynolds number, which is defined as:

$$Re_D = \frac{\rho UD}{\mu}$$

Table 1
Summary of properties for the three graphitic foam specimens tested.

Specimen	Porosity	Average void diameter (μm)	Highest frequency void diameter	k_{eff} (W/m K)
221-1	0.85	410	400	98
219-1	0.90	560	450–500	50
219-2	0.88	400	350–450	65

where U is the fluid velocity measured at the pipe exit, D is the pipe diameter, and ρ and μ are the density and dynamic viscosity of the fluid at the ambient temperature. Though it is only the air velocity that is of interest for the impingement test, the Reynolds number is used here to give an indication of the flow regime.

Since this work seeks to quantify the enhancement obtained by adding layers of GF to the heated surface, the enhancement E is defined as:

$$E = \frac{Nu_{foam}}{Nu_{no\,foam}}$$

to show the enhancement heat transfer obtained by using the GF as an extended surface over the heat transfer measured for the bare aluminum substrate.

4. The experiments

This experimental work has two objectives: to explore the thermal potential of utilizing GF as an extended surface, and to study the relationship between foam thickness/porosity and the resulting enhancement of convective heat transfer.

4.1. Experimental setup

The main test section shown in Fig. 2 consists of a 9.4 cm long, 7.62 cm diameter aluminum cylinder highly insulated on its curved side and one end, and exposed to the impinging air stream at the remaining exposed end. Foam samples were bonded to the exposed end of the aluminum cylinder by Materials Resources International (MRI) using their S-Bond process, a process designed specifically to provide highly conductive bonds between different metallic and graphitic materials. Two 125 W (1.27 cm diameter, 6.35 cm long) cartridge heaters, powered by an AC variable power supply, were friction-fit into holes drilled into the block, as shown in Fig. 3b. To minimize heat loss through the curved wall and the non-exposed end of the aluminum substrate, the cylinder was friction-fit into a 2.54 cm-thick Teflon sleeve, also shown in Fig. 3b. The cylinder was held in the sleeve by a threaded rod that could be used to adjust the position of the substrate such that the heated surface could either be made flush with the end of the Teflon sleeve, or the foam layer could protrude from the sleeve; both conditions were considered in the experiments. The temperature at the bond interface was monitored using three 1.6 mm diameter T-type calibrated thermocouples that were inserted through holes

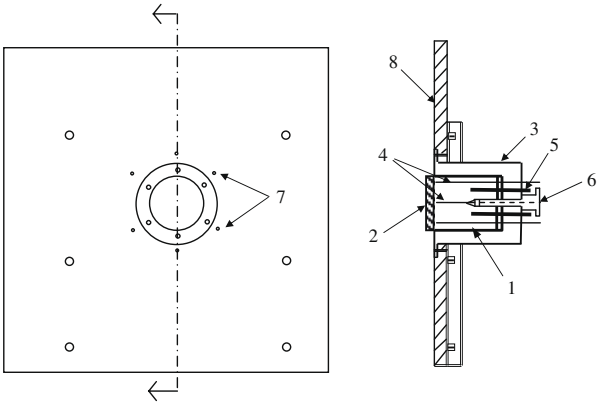

Fig. 2. Cut-away view of the test section showing all components and probes.

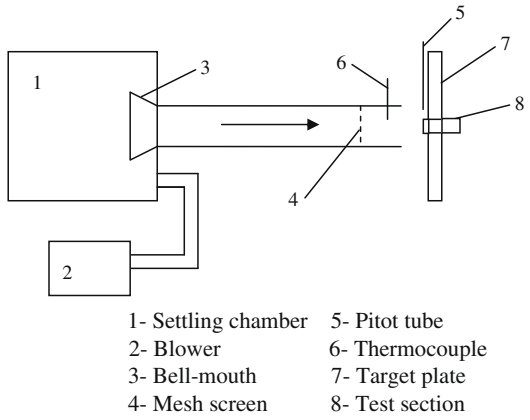

Fig. 3. Schematic view of the experimental setup for the impinging flow experiments.

drilled into the aluminum block to within 1 mm beneath the exposed surface. The entire test section assembly was mounted flush into the surface of a 2.54 cm-thick plywood sheet of dimensions 61 × 61 cm, which was mounted to an adjustable steel frame for support against the impinging air stream.

The impinging air was delivered by a blower that draws air into a settling chamber, where it is conditioned using a stack of air filters, and then passed through a 21.59 cm diameter steel pipe that is 1080 cm (50 diameters) long. The length of the pipe ensures that a fully developed turbulent flow exits the pipe. The free stream air velocity at the exit of the pipe was monitored using a Pitot-tube connected to a barocell pressure transducer and a voltmeter. Mean and rms axial velocity profiles measured with an X-hotwire for one symmetry axis at the pipe exit is reproduced from [10] in Fig. 4. The mean velocity profile, w/W_{jet} (where w is the axial velocity and W_{jet} is the bulk velocity), is compared to a fully developed turbulent flow profile (solid dot). The rms profile w'/W_{jet} (where w' is the axial velocity fluctuation) is also shown in Fig. 4. The structure of the pipe exit air flow is well documented in [10]. Because of the large-diameter pipe used compared to the specimen plan-diameter (also shown at the top of the figure), the exit flow was considered to be effectively uniform across the entire heated surface, thereby

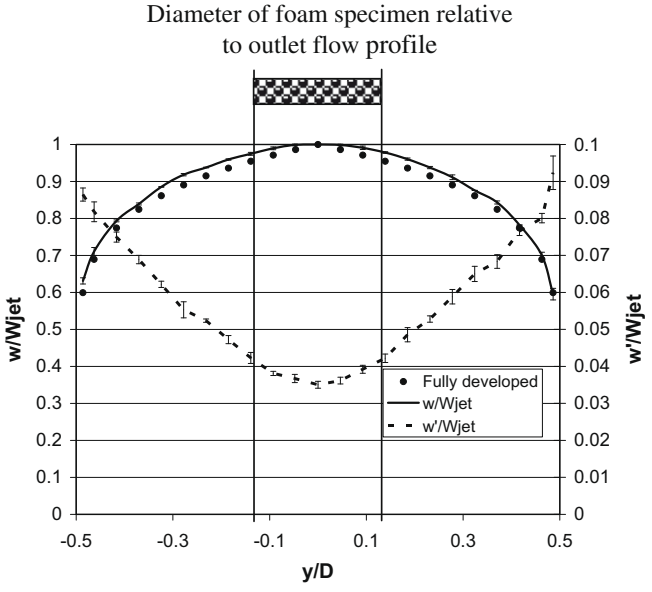

Fig. 4. Axial jet outlet velocity profiles (mean and RMS, error bar in ±1 SD).

removing any influence of the sample position from the pipe exit. A calibrated T-type thermocouple of 3 mm diameter was installed through a hole drilled 5 cm upstream from the pipe exit to measure the air temperature.

The frame supporting the test section was arranged such that the exposed heated surface was perpendicular to the horizontal air-supply pipe, as shown in Fig. 3. The end of the pipe was positioned at a fixed distance of 17.5 cm from the plywood base. Precise alignment of the impinging air stream relative to the test section was done by taking pressure measurements from six pressure taps that were mounted in the plywood sheet in an evenly distributed circular pattern surrounding the heated surface. Adjustments were made to the frame until the pressure readings from the six taps were in balance.

4.2. Test procedure

Tests were conducted for 10, 8, 6, 4, and 2 mm layers of the foam specimens described in Table 1. Experiments were run for 5, 8, and 11 m/s air velocities, corresponding to pipe Reynolds numbers in the range 70,000–160,000, and the power supply was fixed at 60 W. As such, the total number of experiments conducted per foam specimen was 15. For one foam specimen, separate tests were conducted to investigate the effect of having the foam layer protrude from the impingement surface, as opposed to having a completely flush impingement surface. The voltage drop and current drawn by the heaters (used to obtain electrical input energy) as well as all the thermocouples readings were collected using an NI PCI-6014 basic multifunction I/O and NI-DAQ, AMUX-64T Analog Multiplexer data acquisition system that was controlled using a LABVIEW program.

A typical test run started by setting the air speed to the desired value and switching on the cartridge heaters in the test section. The approach to steady-state conditions was monitored using temperature readings from the thermocouples at the heated surface; readings were taken at intervals of 15 min. Once steady-state was reached (typically 4 h), readings of electrical input and all temperatures were recorded in intervals of 1 min for 15 min. The air speed was then adjusted and a similar procedure was used to obtain data for the next air speed. Once tests were complete for 5, 8 and 11 m/s, the aluminum cylinder was removed and the foam layer was machined to the next test thickness. This procedure was continued until tests were conducted for all of the conditions mentioned above. A set of tests was always conducted for the bare substrate once the final layer of foam was removed. Results from this set of tests served as the basis from which to calculate the enhancement obtained using the foam layers.

4.3. Uncertainty

The uncertainty in the present work can be classified to two categories: Reynolds number (or air velocity) and Nusselt number uncertainties. The main uncertainty in the jet Reynolds number is due to the barocell zero setting in the velocity measurement, which is estimated to be less than 2% and this was accounted for in every reading. The uncertainty in the Nusselt number is due to the heat flux input and the target surface temperature measurements. The reading error of the heat input is estimated to be about ±1% and it was essentially cancelled out through the calculation of the relative value of the enhancement parameter E. The largest contribution to the uncertainty in Nusselt number comes from the temperature measurements of the target surface which are estimated to be about ±0.5 °C. On the basis of these uncertainties, the Nusselt numbers computed are accurate to within 5%. The test facility was designed to minimize potential errors in the results. As stated, the main sleeve assembly was constructed from Teflon and insulated from the surroundings using an insulated cover. During the experiments, the cover was not warm to the touch and thus deemed effective in minimizing extraneous heat losses. To further reduce the uncertainty, all reported results are presented as a ratio with respect to the heat transfer of the bare aluminum plate, which was measured using the same procedure as the foam specimens. In this manner, any uncertainty in the input heat flux and heat losses in the test fixture are essentially cancelled out, or at least rendered small relative to other factors.

5. Results and discussion

Results are presented to illustrate the convective heat transfer enhancement, and specifically: to show the impact of the foam surface protruding from the impingement surface, to show the effect of foam thickness, and to show the effect of foam properties.

The effect of foam protrusion is explored because it is of interest to understand the condition that enables the highest infiltration of air into the heated foam. If very little infiltration occurs, little convective enhancement would be expected, whereas if infiltration is high, higher enhancements would also be expected. Fig. 5 compares the heat transfer enhancement obtained with the upper surface of the foam sample flush to the surface of the plywood sheet (flat), and for the whole foam layer protruding above the plywood sheet (extended), both for unconfined impinging flow. The figure shows that the enhancement achieved by the extended foam layers is higher for all foam thicknesses, suggesting that the air infiltration into the foam is higher when the edges of the foam are open and a path exists for infiltrated air to escape. The figure also shows that for the extended foam layers the convective enhancement is higher for thicker layers of foam indicating that the infiltration of air into the cells of the GF is substantial. Enhancements of 30–40% over that of the bare aluminum substrate were measured for extended GF layers of 2–6 mm, respectively. This is 4–12% higher than similar enhancements achieved by setting the foam surface to be flush with the plywood sheet. Fig. 5 also shows that the convective enhancement for the flat cases are essentially independent of foam thickness, suggesting that very little air infiltration occurs when there is no escape route for the infiltrated air. In this case, the heat transfer enhancement is simply due to the larger surface area available at the foam surface (verses the bare aluminum surface). While this result may have been expected, it is of interest to know that the level of enhancement associated with the additional surface area of the GF is 20–28%, depending upon the impingement velocity. This value will depend slightly on the foam porosity, and possibly the solid-phase conductivity. All remaining experiments were conducted for the extended foam condition.

Fig. 6 shows the influence of foam thickness and impingement air speed on convective enhancement for all of the specimens

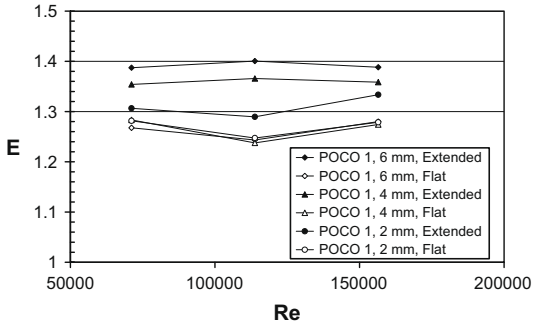

Fig. 5. Plot showing the impact of foam protrusion from the impingement surface on the convective heat transfer enhancement.

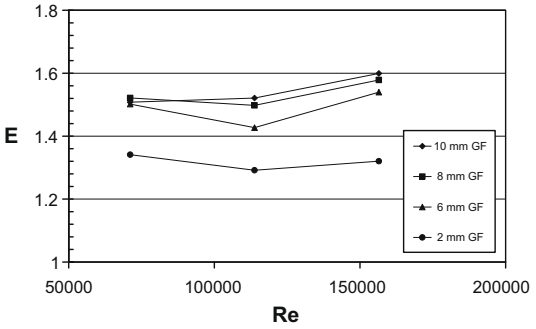

(a) Specimen 219-1

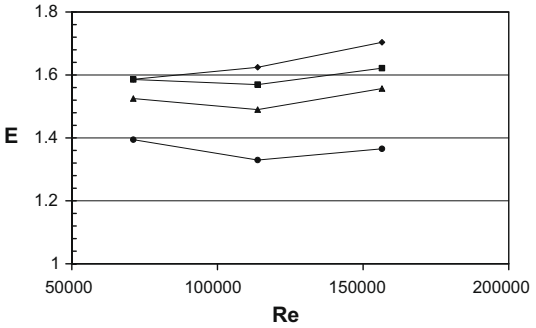

(b) Specimen 219-2

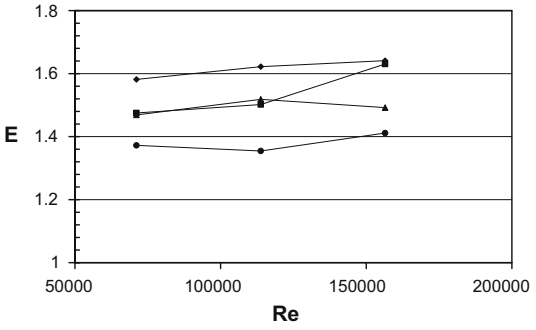

(c) 221-1 foam

Fig. 6. Plots showing the influence of foam thickness on convective enhancement.

shown in Table 1. The plots indicate that enhancements of 30–70% are obtained over the range of air speed considered by varying the thickness of the different foam specimens. In terms of impingement air speed, the enhancement is higher at the highest velocity than the lowest, but for a significant number of the cases shown in Fig. 6, the lowest enhancement was observed at the intermediate air speed. This suggests that for a given foam, the net convective enhancement is due to complementary influences resulting from the increased plan surface area of the foam over the bare substrate, and the exposure to internal surface area for infiltrated air. While the plan surface area is constant for a given foam, the exposure to internal area depends upon the flow condition. Flow through the foam is driven by the pressure gradient set up by the (near) stagnation pressure at the surface and the pressure at the edge of the specimen. Since the influence of the enhanced plan area with *Re* is effectively linear (over the range of *Re* considered), the influence of flow through the foam must be larger at the low air speed. That is, if the trend for the higher air speeds is considered to be increasing linearly due to a continuous increase in the stagnation pressure, then the enhancement at the lowest air speed is higher (for all but 1 condition) than would be predicted by extrapolating backwards from the higher air speeds. This simply implies that the infiltration has a stronger influence on the net convective enhancement at lower flow speeds. A similar phenomena was noted in [4] for the parallel flow condition, where it was argued that the relative amounts of parallel flow verses infiltrated flow affected the trend in the convective enhancement. The difference in this case is that increases in the air speed eventually cause the enhancement to grow due to the higher and higher infiltration of air through the foam. In terms of the foam thickness, the trend for all specimens is that the highest convective enhancement occurs for the thickest foam layers, suggesting that air infiltrates the GF deep beneath the exposed surface. It is also observed that the largest increases occur between 2 and 6–8 mm; in most cases the difference between 8 and 10 mm of GF is relatively small, suggesting that the infiltration limit may be reached for the air speeds considered. Thicker specimens could not be tested due to the limitation of the foam specimens available.

Fig. 7 shows the influence of foam properties on the convective enhancement for all of the air speeds considered. In almost all cases, the 219-2 foam produced the largest enhancement while the 219-1 foam produced the smallest enhancement. On the same basis as that described by Straatman et al. [4], the enhancement is

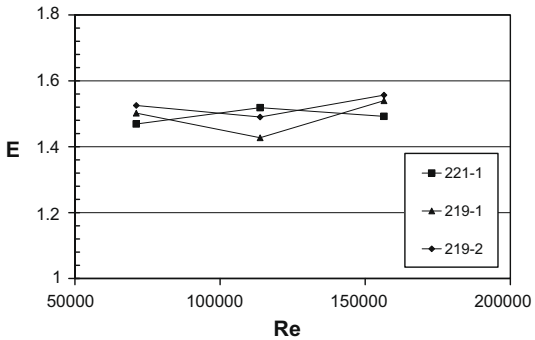

(a) 6 mm thick GF

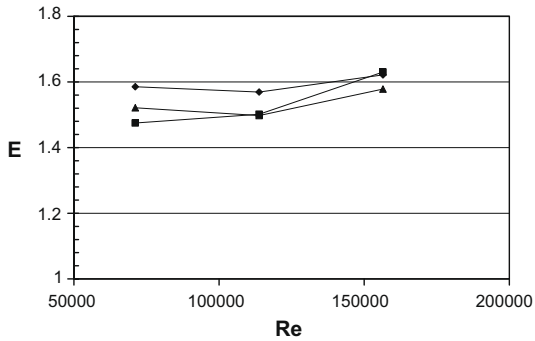

(b) 8 mm thick GF

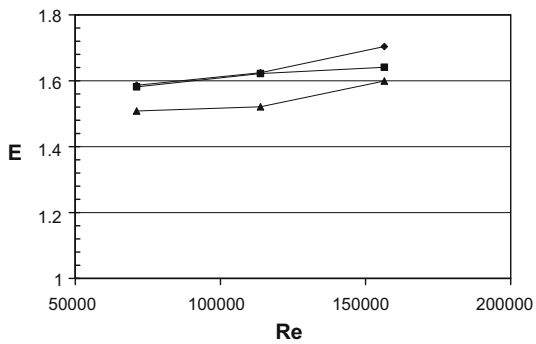

(c) 10 mm thick GF

Fig. 7. Plots showing the influence of foam properties on convective enhancement.

a product of combined effects: the thermal non-equilibrium inside the foam structure, the passage of air into the foam, and the utilization of external and internal surface area (as described above with respect to Fig. 5). The thermal non-equilibrium is driven mainly by the porosity and the solid-phase conductivity of the foam, which in this case is extremely high. Because of the weak infiltration that is expected due to the unconfined nature of the flow, and the high solid-phase conductivities of all of the GF specimens considered, it is likely that the foam is nearly isothermal at the temperature of the substrate and that the conductivity plays a very small role. This was shown to be the case in the parallel flow experiments of Straatman et al. [4] where simultaneous measurements of the substrate and foam surface temperatures showed very little difference. On this basis, the differences between the specimens considered in the present study must be reconciled on the basis of air infiltration and area utilization. As shown in Fig. 1 and described in Section 2, the 219-1 specimen is not ideal for convective enhancement. While the foam structure likely allows substantial infiltration through the large interconnected pores, much of the internal surface area is contained in the smaller pores that are bypassed by the flow, resulting in very poor internal area utilization and, consequently, a poor convective enhancement. The structure of the 221-1 foam would appear to be the most suitable in terms of internal area utilization since the pore structure is effectively homogeneous, however, in comparison to 219-2, the interconnectivity of the cell structure is not high. The 221-1 foam appears to have far fewer cell windows connecting the pores, which leads to a higher hydraulic loss and thus a weaker airflow. The 219-2 foam structure appears to have the best level of interconnectivity of the GF specimens considered, leading to the highest combination of infiltration and internal area utilization, the lowest convective resistance and, thereby, the highest convective enhancement.

6. Conclusions

Three different graphitic foam (GF) specimens were tested in an unconfined impinging airflow arrangement to measure the convective enhancement that is obtainable over that of a bare heated surface. The most significant conclusion is that enhancements of 30–70% were observed for impingement airflows ranging from 7 to 11 m/s and foam thicknesses ranging from 2 to 10 mm. The highest enhancements were observed for GF specimens with the best interconnectivity, as in previous characterization studies. High interconnectivity leads to high air infiltration and high utilization of internal surface area. Future studies will focus on optimization of the foam material and geometric properties for optimal convective enhancement.

Acknowledgements

Authors [a,c] wish to acknowledge the financial support received by the Natural Sciences and Engineering Research Council of Canada. Author [b] wishes to acknowledge support received from the Advanced Automotive Materials Program, DOE Office of FreedomCAR and Vehicle Technology Program, under Contract DE-AC05-00OR22725 with UT-Battelle, LLC.

References

[1] W.J. Klett, R. Hardy, E. Romine, C. Walls, T. Burchell, High-thermal conductivity, mesophase-pitch-derived carbon foam: effect of precursor on structure and properties, Carbon 38 (2000) 953–973.
[2] C.N. Gallego, W.J. Klett, Carbon foams for thermal management, Carbon 41 (2003) 1461–1466.
[3] A.G. Straatman, N.C. Gallego, Q. Yu, L.J. Betchen, B.E. Thompson, Forced convection heat transfer and hydraulic losses in graphitic foam, ASME J. Heat Transfer 129 (9) (2007) 1237–1245.
[4] A.G. Straatman, N.C. Gallego, B.E. Thompson, H. Hangan, Thermal characterization of porous carbon foam – convection in parallel flow, Int. J. Heat Mass Transfer 49 (2006) 1991–1998.
[5] Y. Jayman, A.A. Mohamad, Enhanced heat transfer using porous carbon foam in cross-flow, ASME J. Heat Transfer 129 (6) (2007) 735–742.
[6] T. Jeng, S. Tzeng, Numerical study of confined slot jet impinging on porous metallic foam heat sink, Int. J. Heat Mass Transfer 48 (2005) 4685–4694.
[7] W.H. Hsieh, J.Y. Wu, W.H. Shih, W.C. Chiu, Experimental investigation of heat-transfer characteristics of aluminum-foam heat sinks, Int. J. Heat Mass Transfer 47 (2004) 5149–5157.
[8] W.H. Shih, W.C. Chiu, W.H. Hsieh, Height effect on heat-transfer characteristics of aluminum-foam heat sinks, ASME J. Heat Transfer 128 (2006) 530–537.
[9] Q. Yu, B.E. Thompson, A.G. Straatman, A unit-cube based model for heat transfer and pressure drop in porous carbon foam, ASME J. Heat Transfer 128 (2006) 352–360.
[10] Z. Xu, H. Hangan, Scale, boundary and inlet condition effects on impinging jets with application to downburst simulations, J. Wind Eng. Ind. Aerodyn. 96 (2008) 2383–2402.